KfK 2832/II
Oktober 1979

Fast Rigorous Numerical Method for the Solution of the Anisotropic Neutron Transport Problem and the NITRAN System for Fusion Neutronics Application Part II

A. Takahashi, D. Rusch
Institut für Neutronenphysik und Reaktortechnik

Kernforschungszentrum Karlsruhe

KERNFORSCHUNGSZENTRUM KARLSRUHE

Institut für Neutronenphysik und Reaktortechnik

KFK 2832/II

Fast Rigorous Numerical Method for the Solution of the Anisotropic Neutron Transport Problem and the NITRAN System for Fusion Neutronics Application

Part II

Akito Takahashi[+)] and Detlef Rusch

[+)] Guest scientist from Osaka University, Japan
as a research fellow of the
Alexander-von-Humboldt-Stiftung

Kernforschungszentrum Karlsruhe GmbH, Karlsruhe

Kernforschungszentrum Karlsruhe GmbH
ISSN 0303-4003

Abstract

The I^*-method, which is a non-approximative treatment of the neutron balance equations by the use of double-differential cross sections and a generalized angular transfer probability, is realized within the NITRAN system. It is shown, by means of test calculations for assemblies related to fusion reactor neutronics that double-differential cross section data provide substantial progress in transport problems with kinematically complicated reaction channels like (n,2n), (n,n'γ), and (n,n'α), because the I^*-method is free from kinematic assumptions. The properties of the exponential method to generate the supplementary equations to the S_N equations are investigated.

Schnelle strenge numerische Methode für anisotrope Neutronentransport-Rechnungen und das NITRAN-System für Anwendungen bei Neutronik-Rechnungen zu Fusionsreaktoren

Zusammenfassung

Die I^*-Methode, die eine strenge Behandlung der Neutronen-Bilanzgleichungen durch den Gebrauch doppelt-differentieller Wirkungsquerschnitte und einer generalisierten Winkel-Übergangswahrscheinlichkeit ist, wurde innerhalb des NITRAN-Systems verwirklicht. Mit Hilfe von ersten Rechnungen zu Neutronentransport-Problemen des Fusionsreaktors wird gezeigt, daß doppelt-differentielle Wirkungsquerschnitte bei kinematisch komplizierten Reaktionskanälen wie (n,2n), (n,n'γ), (n,n'α) deutlich von Vorteil sind, weil die I^*-Methode frei von kinematischen Annahmen ist. Die Eigenschaften der exponentiellen Methode zur Erzeugung der Ergänzungsgleichungen zu den S_N-Gleichungen werden untersucht.

Contents

Preface

The present report is written as a strict continuation of KFK 2832, Part I, "Fast Rigorous[+)] Numerical Method for the Solution of the Anisotropic Neutron Transport Problem and the NITRAN System for Fusion Neutronics Application". In part I two new methods, the Ii- and the I*-method, are introduced. The Ii-method, which relies on existing nuclear data files, was realized by means of the code system NITRAN. At that stage of the development the NITRAN system comprised one-dimensional transport calculations in spherical geometry with only one isotope and a single material zone. Having proved that this method is suited for technical use, the improvement of the code system with respect to this point is a necessary conclusion. This is one aspect this part II on the NITRAN system deals with.

The main aspect of this part II is the practical introduction of the I*-method, which is based on the following argumentation: A considerable amount of the calculational efforts is devoted to the reconstruction of the three-dimensional scattering kernel matrices from the existing single-differential data files. As this can be done independently from the transport calculation, the separation of the kernel and the transport calculations is already an essential part of the Ii-method. But it is more effective to avoid this reconstruction of the scattering kernel matrices at all and to pass over to the use of double-differential total neutron emission cross sections from a new type of evaluated data file, together with a generalized angular transfer probability matrix. In this part II we want to present the distinct advantages of the I*-method, which uses these data, by means of calculational results.

Before reading this part II, it is recommended to read part I, because the definitions and the formulae are not repeated herein.

+) Rigorous: non-approximative treatment of the neutron balance equations.

1. Introduction

Radiation transport calculations need only two types of nuclear data: the total cross section and the double differential total secondary emission cross section as the scattering kernel in the integro-differential transport equation. Since the latter requires a large storage area, if the energy and angle coordinates are subdivided into sufficiently narrow intervals, and since the transformation of the coordinate angles to the scattering angle introduces complexity, approximations have been used. The accuracy of the approximations increased according to the requirements of the transport calculations. The basic approximation is the isotropic scattering. There we need only energy distributions for sedondary neutrons as differential data[+)]. The next step in the series of approximations is the T_1, the so-called transport approximation, which needs only the average cosine of the scattering angle as additional information on the distribution of secondary particles. After this, a more precise method was developed, the P_L method /1/, which uses truncated Legendre polynomial series to approximate the scattering kernel. The data needed to realize the P_L method are partial cross sections with either energy or angle distributions for the secondary particles in single-differential form, which are treated with use of kinematic relations to reconstruct the double differential cross section of the scattering kernel. An improvement of the P_L method is the T_{L+1} method /2/, which takes the estimation of the rest of the Legendre series into account in a consistent manner. The latter two methods save computer space by storing coefficients of series expansions rather than point data. Both start from disturbed radiation balance equations in a microscopic sense. Since storage capacity in modern computers is no langer a severely limiting factor, the rigorous,

---

+) Sometimes cross sections for inelastic scattering with excitation of discrete levels are called "differential". We do not continue this habit, but apply the term "partial" for all cross sections which describe the incident energy dependence of a certain reaction channel.

i. e. non-approximative methods based on an undisturbed microscopic neutron balance equation can be introduced. From the programming point of view these methods replace evaluations of series (which means calculating) by use of stored data in sufficiently subdivided form (which means table-look-up).

In neutron transport calculations in general only the anisotropy of the elastic scattering is included for the calculations. But there is experimental evidence /3/, /4/, /5/ that for fusion reactor calculations the anisotropy of the nonelastic scattering must be taken into account. The status of the evaluated nuclear data files, of course, is such that the requirements of the currently accepted approximations is met. At present this is the single-differential form of partial cross sections. Using this form of evaluated nuclear data for a rigorous transport calculation means that one has to reconstruct the complete particle emission from the scattering center as a function of the incident energy and the outgoing energy and angles in the laboratory system. In the Ii-method /6/ this is done by means of the collision kinematics and the rigorous angular transfer probability for each partial cross section. With 14 MeV source neutrons this reconstruction process comprises already so many reaction channels that it is inefficient to repeat this for each transport calculation. Therefore, the scattering kernel matrices are stored on magnetic tape. This is nothing but another evaluation of evaluated data. Moreover, by separating the experimental information on the scattering into partial cross sections and recombining them for the transport calculations necessary double-differential information is destroyed and additionally, by loosing covariance information, the probable errors of the result will be increased. Therefore, inversely, if a certain target accuracy of the results is to be met, the present practice raises the demands for the error margins of the original experimental results unduly /7/. The most prominent example with respect to this problem is the nuclear data for beryllium, for which material double-differential data have been published /8/. More double-differential data are being accumulated /9/. To stimulate an efficient use of these data is one of the intentions for this paper: The I*-method, which

uses these data, is realized by means of new data processing codes and the transport calculations are performed with improved and extended versions of the NITRAN system codes, ref. /6/.

For abbreviation the expression "double-differential cross section data" will be referred as "DDX data".

The lay-out of the NITRAN system for the I*-method is still that of ref. /6/, the actual version is explained in section 2. The subcodes for the new parts of the system are explained in section 3. In section 4 the advantages of the I*-method are illustrated by comparison with another approach. In section 5 we present results of some test calculations related to the neutronics of the fusion reactor for Be, a Be-Li mixture, and an assembly with Be and Li in separate material zones. The implications of these results are discussed in section 6. Technical extensions and improvements of the "old" NITRAN codes are reported in appendices.

2. The extended NITRAN system

The extended NITRAN system comprises both the Ii- and the I*-method. The lay-out of this system is shown in Fig. 1. Possible flows ("routes") are drawn for the Ii- and the I*-method. The Ii-route has been explained in ref. /6/, and has been completed with the code NIMIX, which is for mixing isotope kernels and arranging them in the order of the material zones in an assembly. Details are given in Appendix 2 . The transport codes NITRAN-MP (for Multilayer Plane geometry, one-dimensional) and NITRAN-MS (Multilayer Sphere geometry) are also new and they are explained in Appendices 3 and 4. Some improvements in NIKER and the transport codes are mentioned in the Appendix 1, they are merely technical. Several trial calculations were carried out with use of supplementary equations derived from an exponential interpolation of the fluxes /10/, /11/. The merits of the exponential method (EM) are low for the case of a monoenergetic source in the spherical geometry. It fails to interpolate the angular fluxes in the angle space,

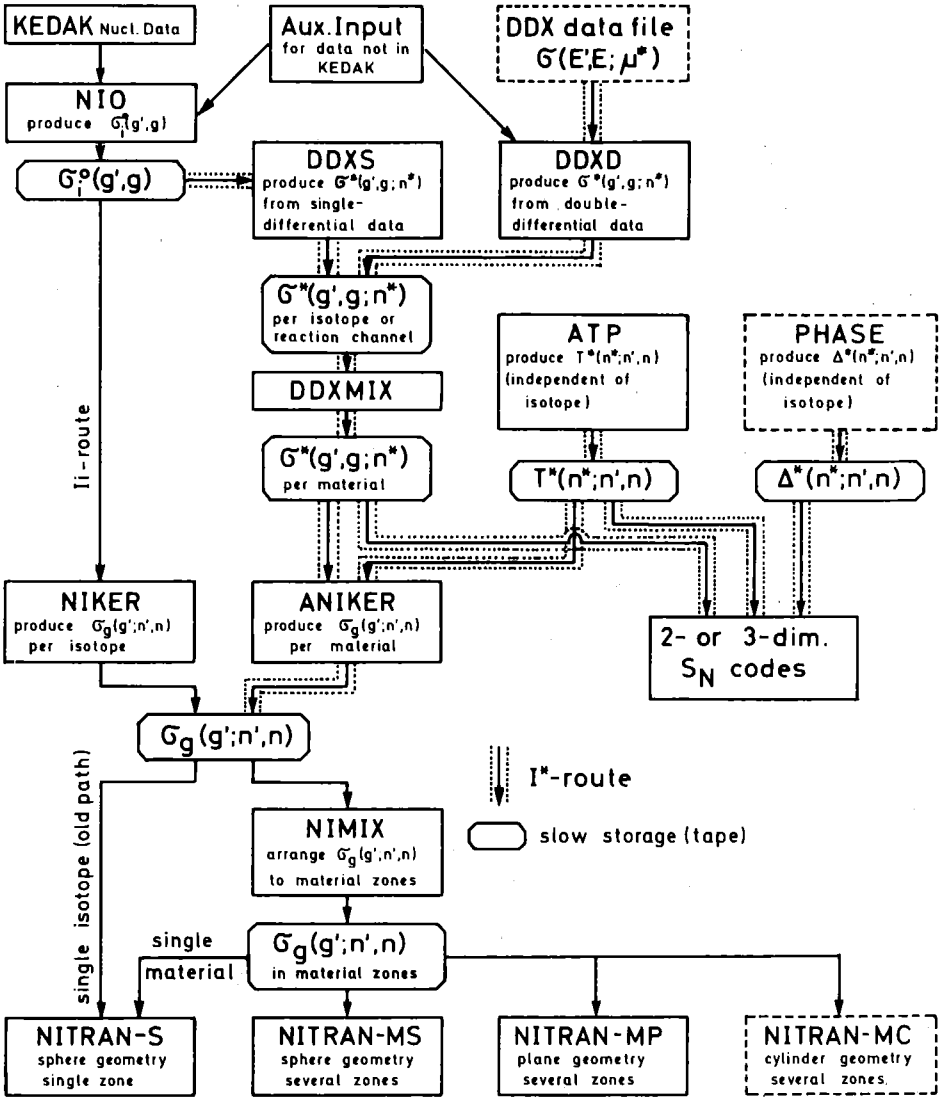

Fig. 1: Concept of the extended NITRAN system realizing the I*-method

where the angular fluxes vary by orders of magnitude from one meshpoint to the next. For a discussion of this problem see Appendix 4. The I*-route (in Fig. 1: DDXD or DDXS → DDXMIX → ATP+ANIKER → S_N) is new. In the future the main flow will be from DDX data. Actually it is only an auxiliary input from cards. DDXD produces the grouped (averaged within energy and scattering angle interval) double-differential cross sections (double-differential with

respect to the outcoming energy and scattering angle) for each material or isotope, whichever is available from the data base. The program DDXS does the same for the single-differential data with use of the reaction kinematics. The input is not directly from the data base, but from NIO, where the P_o kernels are written on magnetic tape. For mixtures of material the program DDXMIX combines the grouped DDX. Compared to the Ii-route, much less computer space is needed for these operations. In section 3 this is explained more detailed.

Grouped data from either DDXD or DDXS are written on magnetic tape. For one-dimensional calculations the program ANIKER produces the scattering kernel matrices with use of the generalized angular transfer probability $T^*(n^*;n',n)$, which is generated by the program ATP. The route to two- or three-dimensional S_N calculations is not yet open. There the scattering phase matrix has to be produced by a program "PHASE" and the S_N equations have to be solved by appropriate codes. The storage of intermediate data on magnetic tape is based on the same idea as in the initial NITRAN system: avoid unnecessary repetitions of calculations.

In the Ii-method the kinematics and the angular transfer probability $Ii(\mu',\mu)$ are used to reconstruct the scattering kernel, i. e. the relation between an incoming and an outgoing particle current at a scattering center with no distinction between the various reaction types in the final result. By the formulation of this process it becomes less obvious that one deals with a reconstruction. When entering the I^*-route from the DDXS path this is more easily recognized. The hybrid use of the ideas of the Ii- and the I^*-method opens the chance to demonstrate the usefulness of genuine DDX data and allows a smooth transition to the new data type.

We have the possibility to use DDXD and DDXS in a mixed mode, if some data for particular reaction channels are given as single-differential data (SDX) and others as DDX. This was practiced for the test calculations described in section 5. For one-dimensional calculations the code NIMIX can also be used to arrange the scattering kernel matrices for several layers of material.

In the I*-route calculations of the (anisotropic) scattering kernel matrix $\sigma_g(g';n',n)$ are carried out with use of the Eq. (80) in ref. /6/, which is+)

$$G_g(g';n',n) = \sum_{n_1^*}^{n_2^*} G^*(g',g;n^*) \cdot T^*(n^*;n',n) \cdot W_{n^*} \tag{1}$$

3. Subcodes in the I*-route for the scattering kernel production

3.1 ATP

The subcode ATP produces a numerical table of the generalized angular transfer probability following the averaging formula for the I*-function.

$$T^*(n^*;n',n) = \int_{\Delta\mu}\int_{\Delta\mu'}\int_{\Delta\mu^*} I^*(\mu^*;\mu',\mu)\, d\mu^*\, d\mu'\, d\mu \Big/ (\Delta\mu^* \cdot \Delta\mu' \cdot \Delta\mu) = \tag{2}$$

$$= \int_{\Delta\mu}\int_{\Delta\mu'} \left[\arcsin y_{n^*+\frac{1}{2}} - \arcsin y_{n^*-\frac{1}{2}}\right] d\mu'\, d\mu \Big/ \left(\pi \cdot \Delta\mu^* \Delta\mu' \cdot \Delta\mu\right) \tag{3}$$

with

$$y_{n^*\pm\frac{1}{2}} = \frac{\mu^*_{n\pm\frac{1}{2}} - \mu_{n'}\mu_n}{\sqrt{1-\mu_n^2}\sqrt{1-\mu_{n'}^2}}; \quad \text{for } \beta_1^* < \mu^*_{n\pm\frac{1}{2}} < \beta_2^* \tag{4}$$

$\mu^*_{n\pm\frac{1}{2}}$ = boundaries of the angular interval $\Delta\mu^*_n$

In ref. /6/ the averaging over μ^* was replaced by the point value at $\mu=n^*$. Here we deal with the full averaging over the three variables.

In some special cases we have

$$y_{n^*-\frac{1}{2}} = -1 \quad \text{for } \mu^*_{n-\frac{1}{2}} < \beta_1^* < \mu^*_{n+\frac{1}{2}} < \beta_2^* \tag{5}$$

$$y_{n^*+\frac{1}{2}} = +1 \quad \text{for } \beta_1^* < \mu^*_{n-\frac{1}{2}} < \beta_2^* < \mu^*_{n+\frac{1}{2}} \tag{6}$$

$$y_{n^*\pm\frac{1}{2}} = 0 \quad \text{for } \mu^*_{n+\frac{1}{2}} < \beta_1^* \text{ or } \beta_2^* < \mu^*_{n-\frac{1}{2}} \tag{7}$$

+) In contrast with ref. /6/ the designation "σ^*" is now used for $\sigma^*(g',g;n^*)$ only. This characterizes its importance in the I*-method, whereas $\sigma_g(g';n',n)$ is common to both the Ii- and the I*-method (see fig. 1.).

where from Eq. (2) to (7)

$$\beta_1^* = \mu_n\mu_{n'} - \sqrt{1-\mu_n^2}\cdot\sqrt{1-\mu_{n'}^2}\,; \quad \beta_2^* = \mu_n\mu_{n'} + \sqrt{1-\mu_n^2}\cdot\sqrt{1-\mu_{n'}^2} \tag{8}$$

The flow chart of the code ATP is shown in Fig. 2. As "calculational conditions" we read NMAX, KMAX and the μ_n-set from cards. NMAX is the order

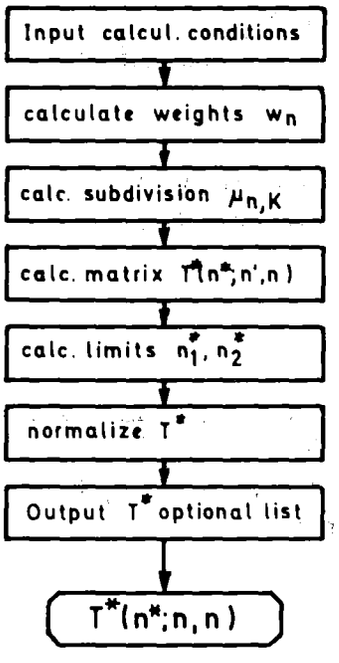

Fig. 2: Flow chart of ATP

of S_N, KMAX the number of subdivisions within the angular intervals $[\mu_{n-1},\mu_n]$. Practically sufficient accuracy was obtained with KMAX = 10 in S_{19} calculations.

There is no severe problem associated with this code if one does not forget the switching between the conditions (4) to (7). Angular transfer matrices $T^*(n^*;n',n)$, normalized with

$$\sum_{n_1^*}^{n_2^*} T^*(n^*;n',n)\cdot w_{n^*} = 1 \tag{9}$$

are stored on magnetic tape together with n_1^* and n_2^*, which correspond to β_1^* and β_2^*.

An example for T^* is shown in Fig. 3.

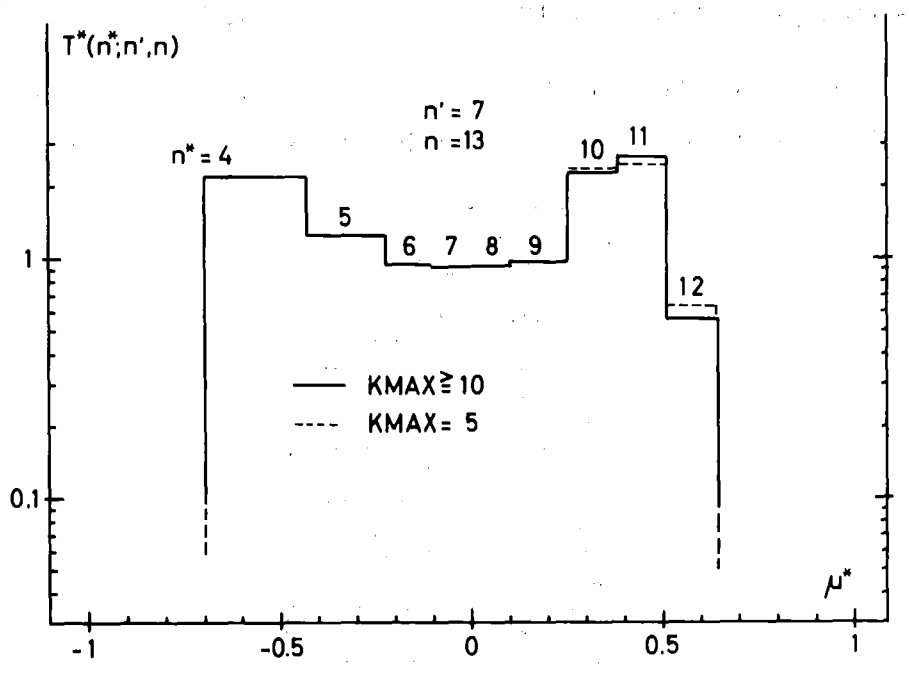

Fig. 3: Example of discretized angular transfer probability for the μ_n set S_{19}

3.2 DDXD

This is the code to produce grouped DDX data from a DDX data base. The original data are interpolated and averaged by means of the following formula, which is Eq. (81) of ref. /6/:

$$\sigma^*(g';g;n^*) = \left[\int_{\Delta E_{g'}} f_w(E') \int_{\Delta E_g} \int_{\Delta\mu_n^*} \sigma(E',E;\mu^*)\, d\mu^*\, dE\, dE'\right] \Big/ \left[\Delta\mu_n^* \int_{\Delta E_{g'}} f_w(E')\, dE'\right] \quad (10)$$

The weighting function $f_w(E)$ can be generated in the traditional way. The flow chart of DDXD is shown in Fig. 4.

The actual input to DDXD is from cards, because we do not possess DDX data (not even formally) in a standard data base. Such data for ^{9}Be at three inci-

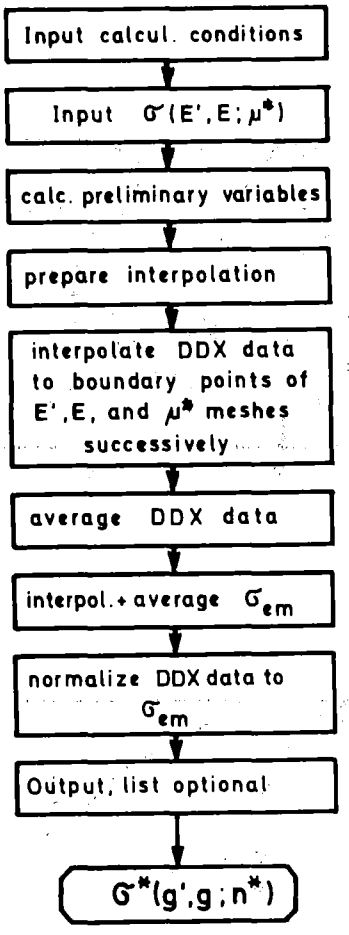

Fig. 4: Flow chart of DDXD

dent neutron energies are the only published ones which we found and they were used for the test calculations, see section 5. Presently DDXD uses linear interpolation and, for completeness, extrapolation. Improvement by using more sophisticated functions (e. g. Spline functions) should be introduced carefully, because their use is not trivial /12/.

DDXD passes with the interpolation through the arrays of g', g, and then n^*. Averaging is performed and the grouped data are renormalized for numerical consistency to the total neutron emission cross section $\sigma_{em}(g')$ with the following condition:

$$\sum_{n^*} \sum_{g} \sigma^*(g',g;n^*) W_{n^*} = \sigma_{em}(g') \qquad (11)$$

$\sigma_{em}(g')$ is also read from the auxiliary card input. The final data are listed and stored on magnetic tape in the order of the sink energy group. Examples of the grouped DDX data for ^{9}Be, derived from the original data in ref. /8/, are given in Fig. 5.

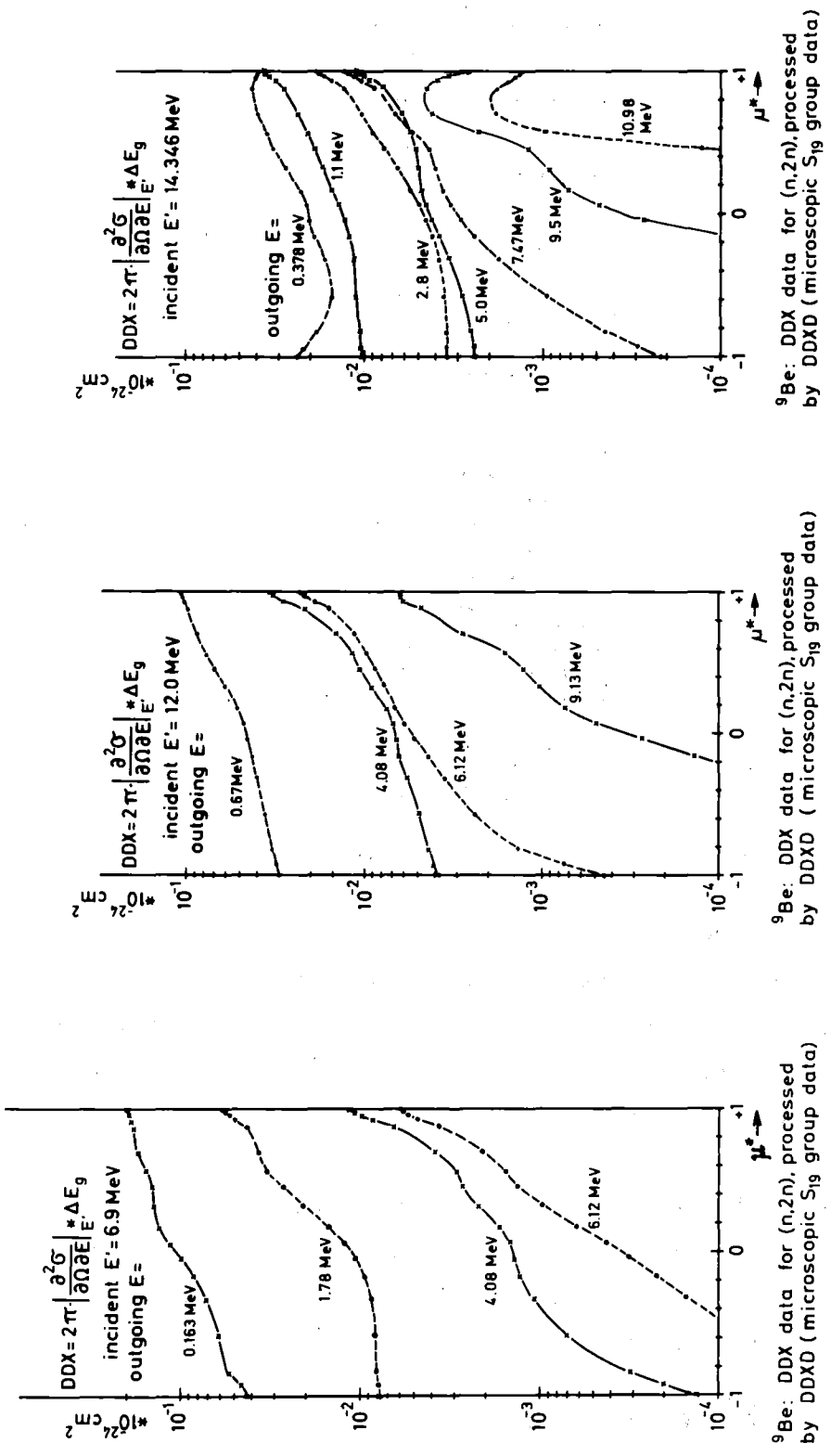

Fig. 5: Example of DDX data for ^{9}Be, processed by DDXD

3.3 DDXS

This code produces grouped DDX data for an isotope from a single-differential cross section (SDX) data base. Since the structure of such a code, if started from scratch, would have to contain many elements of the code NIO, such as reading data, interpolation and grouping, generating secondary distributions, we save some work by starting from the P_o kernels produced by NIO. Then we are faced with one type of single-differential data only. We named the trial code DDXS-T in order not to spoil the more general name DDXS, in case that there should show up severe limitations of this concept.

The flow chart of DDXS-T is shown in Fig. 6. As the output of NIO is used as input, the sequence of the data processing is the same as in NIKER. First the production of DDX data is executed for elastic scattering (L=1), then for inelastic level scattering (L=2...LMAX), and finally for the scattering to the continuum, which is including (n,2n) and (n,3n).

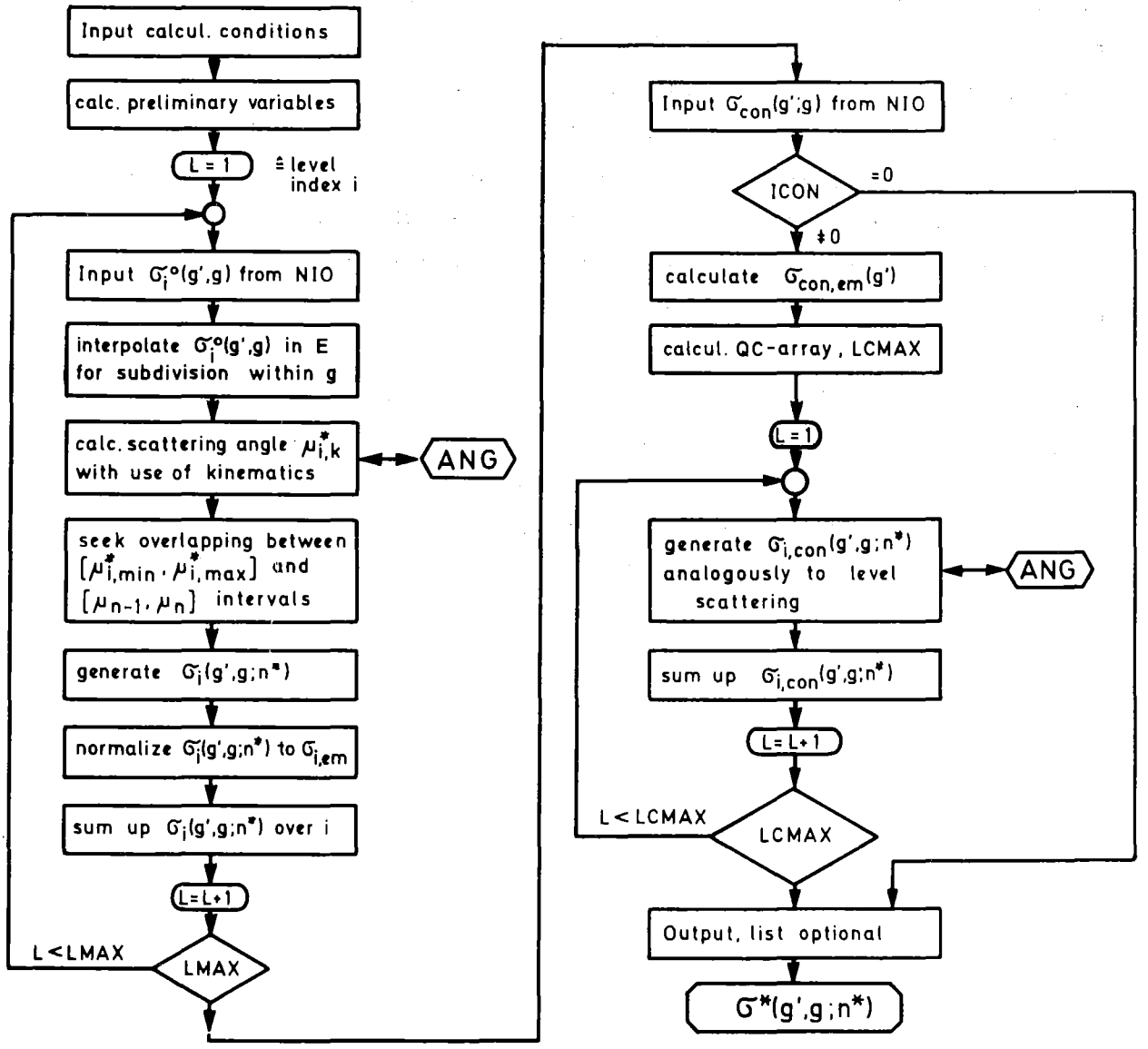

Fig. 6: **Flow chart of DDXS(-T)**

Inside the loop of the sink energy group g (outgoing energy) the scattering angle μ_i^*, which corresponds to scattering from $E_{g'}$ to E_g, is calculated using the kinematic equation Eq. (9) of ref. /6/:

$$\mu_i^* = \frac{1}{2}\left\{(A+1)\sqrt{\frac{E_g}{E_{g'}}} - \frac{1}{A+1}\sqrt{\frac{E_{g'}}{E_g}}\left[A^2\left(1-\frac{Q_i}{E^*}\right)-1\right]\right\} \qquad (12)$$

This is performed in subroutine ANG. For the energy groups g' and g the transformation of the energy variables E' and E within the intervals into μ_i^* results in an interval, the limits of which are named $\mu_{i\,min}^*$ and $\mu_{i\,max}^*$. To find these limits, the search is done by evaluating Eq. (12) for the subdivision points (KMAX) within both groups. The interval $[\mu_{i\,min}^*, \mu_{i\,max}^*]$ is either partly or entirely falling into intervals of the set μ_n^* for the transport calculation. So, when adding up the parts of the P_o kernel, which contribute to a particular interval $[\mu_{n-1}^*, \mu_n^*]$, we have to seek for the fraction, with which both intervals overlap. Fig. 7 illustrates the five possible cases.

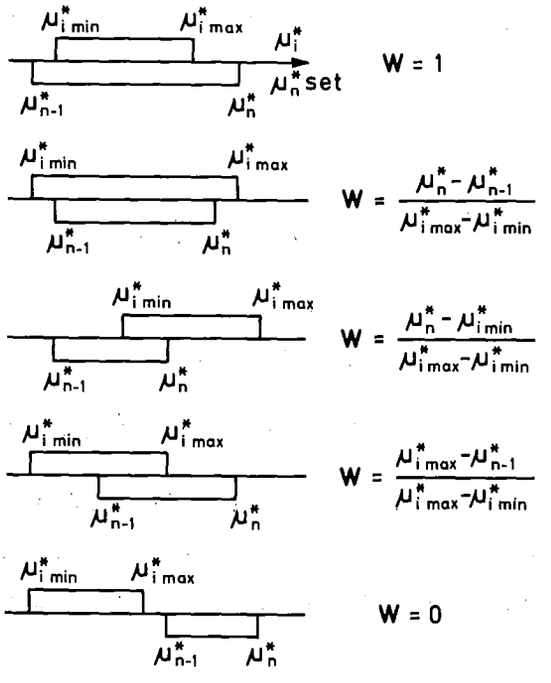

Fig. 7: The five cases of overlap between the intervals of μ_i^* and μ_n^*

We have for the scattering probabilities

$$\sigma_i(g',g;n^*) = \sum_{g'} \sum_{g} \sigma_i^{\circ}(g',g) \cdot W_{g'g}(\Delta\mu_i^*, \Delta\mu_n^*) \qquad (13)$$

$\Delta\mu_n^*$ is the width of the interval.
In this equation $W_{g',g}/\Delta\mu_n^*$ is the fraction with which both intervals overlap. Many of the $W_{g',g}$ will be zero. The scanning for the non-zero values need not be extended over the entire range of g' and g, because the kinematic limitation for the reaction channel i is already known from NIO, where this information (LIMIN, LIMAX, JISHO, JIMAX) is used to reduce storage area and computing time. At this stage of the problem the process to get grouped DDX is similar to the method described in ref. /13/, but there it is applied only for elastic scattering. At later stages the methods differ.

Again as in NIKER the kinematics in the energy range between the forward and the backward threshold are simplified to use only the positive sign of the root in the solution of the equation for μ_i^*. The $\sigma_i(g',g;n^*)$ obtained with Eq. (13) is normalized for numerical consistency to the total neutron emission cross section for the particular reaction type i, which is

$$\sigma_{i,em}(g') = \sum_{g} \sigma_i^{\circ}(g',g) \qquad (14)$$

Thus:

$$\sum_{g} \sum_{n^*} \sigma_i(g',g;n^*)\, w_{n^*} = \sigma_{i,em}(g') \qquad (15)$$

The main difference between NIKER and DDXS is the explicit output of $\sigma^*(g',g;n^*)$ in DDXS, whereas in NIKER this is bypassed by directly generating

$$\sum_{n^*} \sigma^*(g',g;n^*) \cdot T^*(n^*;n',n) \cdot w_{n^*} \equiv \sigma_g(g';n',n). \qquad (16)$$

Therefore the additional discretization step is needed in DDXS. The advantage of the I^*-method to require less storage capacity for the kernels is paid with the slight disadvantage of the additional discretization step when starting from a single-differential data base. This, however, is not the true aim of the I^*-method.

As already stated in ref. /6/, section 3.3.2 on NIKER, the I*-method does not present the difficulties as the Ii-method for heavier nuclei. If the P_o kernels are given in fine groups for the outcoming energy, DDXS presents no difficulties to transform the energy coordinate into the μ_i^* coordinate. At present, in the code DDXS-T we assume that the group structure for incoming energy and outgoing energy are identical. This is also assumed in NIO. To eliminate this limiting assumption is a necessary improvement of the codes to be done next.

Analogously to NIKER the $\sigma_i(g',g;n^*)$ are summed up for the elastic and level scattering to give $\sigma_{level}(g',g;n^*)$. Then the continuum scattering is treated, again analogously to NIKER, with the Q_c array as in NIKER give $\sigma_{con}(g',g;n^*)$. So, finally we have the grouped total neutron emission double-differential cross section+):

$$\sigma^*(g',g;n^*) = \sigma_{level}(g',g;n^*) + \sigma_{con}(g',g;n^*). \qquad (17)$$

The output is stored on magnetic tape.

3.4 DDXMIX

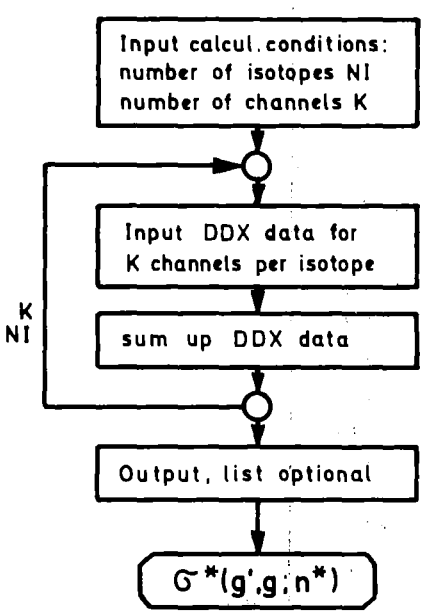

Fig. 8: Flow chart of DDXMIX

+) A shorter name for this should be introduced. Unfortunately, the term "transport cross section" is used for the T_1 approximation.

This is an interface program to arrange the grouped DDX data of the isotopes for materials of several isotopes. There is no need for exciting know-how in this code, as can be seen from the flow chart in Fig. 8.

The present code needs not to arrange the data for several layers of material, because this can be done with NIMIX. On the other hand DDXMIX has to combine DDX data for various reaction channels of the same isotope, if partially data are available from a DDX data base and only the rest has to be reconstructed from a SDX data base. This option was used for the data of ^{9}Be, where we had DDX data for (n,2n) from ref. /8/ and the rest from KEDAK /14/. This operation is not at all difficult, because the data for a fraction of the possible reaction channels are treated as coming from another isotope.

Examples for grouped DDX data are given in Fig. 9.

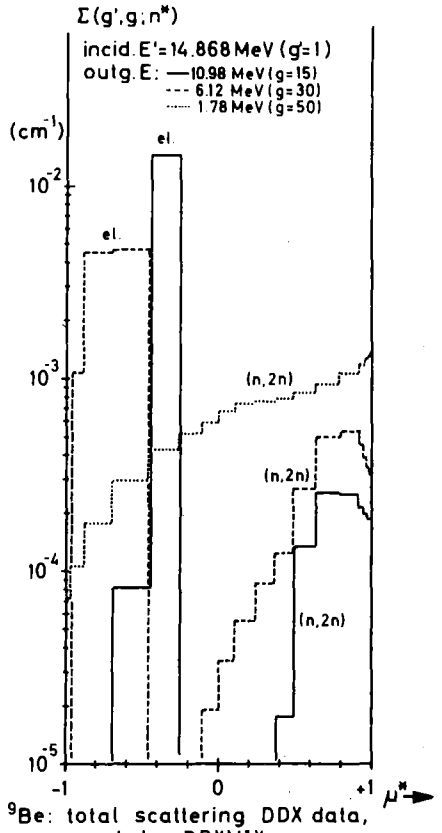

Fig. 9: ^{9}Be: total scattering DDX data, processed by DDXMIX

3.5 ANIKER

This is the subcode to produce the scattering kernel matrices for the one-dimensional transport calculation using Eq. (1). The inputs are the grouped DDX data from either DDXMIX or from DDXD or DDXS directly, and the angular transfer probability matrix from ATP. The code is so simple that explanations beyond the flow chart in Fig. 10 are not needed. The output is stored on magnetic tape in the order of the sink energy group.

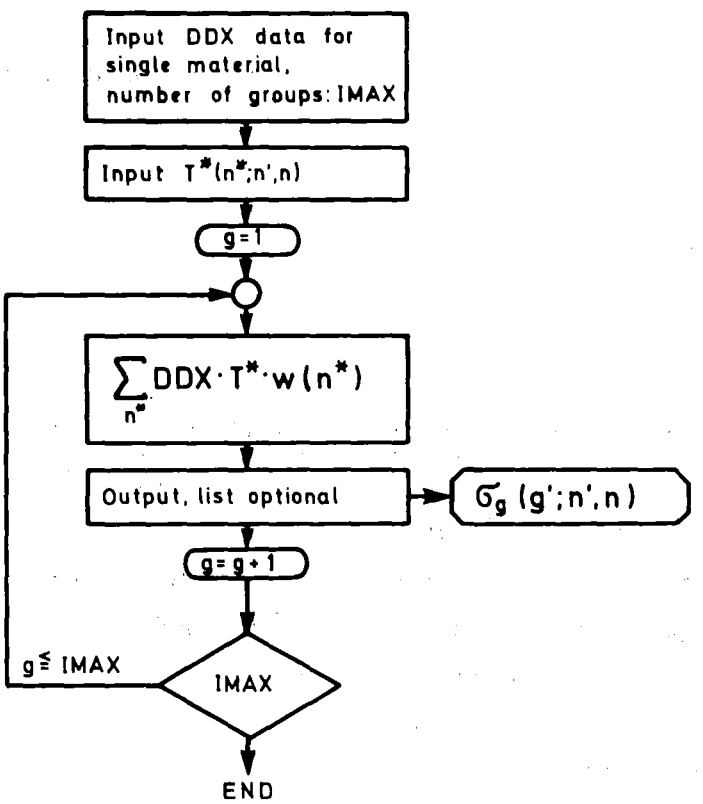

Fig. 10: Flow chart of ANIKER

4. Comparison between the I*-method and two other approaches

4.1 Direct method

In ref. /13/ a calculational concept is proposed which also allows the direct numerical integration of the collision source term. For this approach they found that "the transfer cross sections must be evaluated for all transfer angle combinations $\{\mu_{ij} \rightarrow \mu_{k\ell}\}$. Such considerations necessitate large data storage requirements, and computer storage limitations often preclude the use of this technique". This statement, however, does not apply to the I*-method. A more close look at the calculational flow in both methods reveals the origin of this difference, which is decisive for the practical use.

The loop organization of the direct method proposed in ref. /13/ is as follows:

```
DO 2    μ
DO 2    φ
   collision source = 0
DO 1    μ'
DO 1    φ'
   calculate scattering angle μ* (≙ μ_o in ref. /13/) with
   μ* = μμ' + √(1-μ'²) · √(1-μ²) · cos (φ'-φ).
   discretize μ* into μ_n
   seek σ(g',g;μ*)within appropriate interval of μ*
   (continuous data in the μ*-variable)
   calculate collision source
1 CONTINUE
2 CONTINUE
```

The loop organization of the I*-method is not much different from that:

```
DO 2    μ
DO 2    φ
   collision source = 0
DO 1    μ'
DO 1    μ* with limitation β1* and β2*        ←
   read tables T* and Δ*                      ←
   calculate collision source term with use of grouped DDX data
   (averaged also in μ*)                      ←
1 CONTINUE
2 CONTINUE
```

The arrows point to the essential parts of the loop organization. The I^*-method gives a more strict discretization by the use of the generalized angular transfer probability. This allows to discretize the DDX data prior to the very transport calculations (e. g. the solution of the S_N equations or the Monte Carlo calculation). This distinct calculational advantage for two- or three-dimensional calculations is enhanced by the limitation for the execution of the innermost DO-loop for μ^*. In the I^*-method this loop is executed for the non-zero values of the transfer cross section only, whereas in the direct method these values must be seeked within the execution of the loop.

For one-dimensional calculations the difference between both methods becomes smaller, but is still large enough to make the I^*-method superior. The integration of the kernel over an arbitrary phase shift Δ can be executed in the I^*-method as well as in the direct method, though this is not mentioned in ref. /13/.

4.2 Calculational speed compared to the P_L method for the two- or three-dimensional case

Let us consider a S_{19}-P_5 calculation for a duct problem. There we have to sum up 25 terms of the series expansion in the collision source term calculation. In the I^*-method with its limitation in the innermost DO-loop for μ^* we need a summation of only about 10 terms or less, and for each of these terms less calculational time is needed than for the series calculations. So in total the calculational speed of the I^*-method for two- or three-dimensional calculations is several times higher than that of a S_N-P_L calculation.

Additionally it remains questionable, wether a P_L calculation for a duct problem is appropriate.

5. Test calculations and their results

^{9}Be is the most prominent example for the need of genuine double-differential total neutron emission data for accurate transport calculations. Recently another verification of the discrepancies between measured and calculated multiplication factors of a beryllium layer has been reported /3/, which confirms the older results /15/. They found that the calculation predicts twice as many additional neutrons as were found in the experiment. In ref. /6/ we discussed the origin of that discrepancy. Here we report numerical results for some assemblies containing beryllium.

5.1 Calculational conditions and nuclear data

In the present calculations an asymmetric μ_n set /5/ of 19 points, see Table 1, was used. While the results are close to those of a S_{32} calculation with a symmetric μ_n set (see Table 2 in ref. /6/), calculational time was saved. The 67 energy group structure of ref. /6/ was retained. Data for the elastic scattering on ^{9}Be were taken from KEDAK /14/, single-differential data on (n,2n) from ENDF/B-IV, processed by SPTG-4Z /16/ (an extension of SUPERTOG /17/). DDX data for (n,2n) from ref. /8/ are given down to .4 MeV. As this is already well below the maximum of the evaporation part of the secondary neutron spectra, the data were interpolated linearly between the lowest value and zero. For ^{7}Li the same data as in ref. /6/ were used.

For all calculations the elastic scattering was treated anisotropically. For the nonelastic scattering matrices of single-differential origin the calculation was made with isotropic scattering in the lab. system as is usually done. Examples for the scattering kernels are given in Fig. 11. The data are integrated over the scattering angle μ^{*}. As can be seen from Fig. 11, the (n,2n) data from ENDF/B-IV yield more neutrons in the energy range 3 to 13 MeV than the double differential data.

How this difference affects neutron fluxes and neutron multiplication is shown in the next section.

For the calculations of the neutron transport in Be-Li-mixed assemblies the nonelastic scattering was treated either isotropically or anisotropically

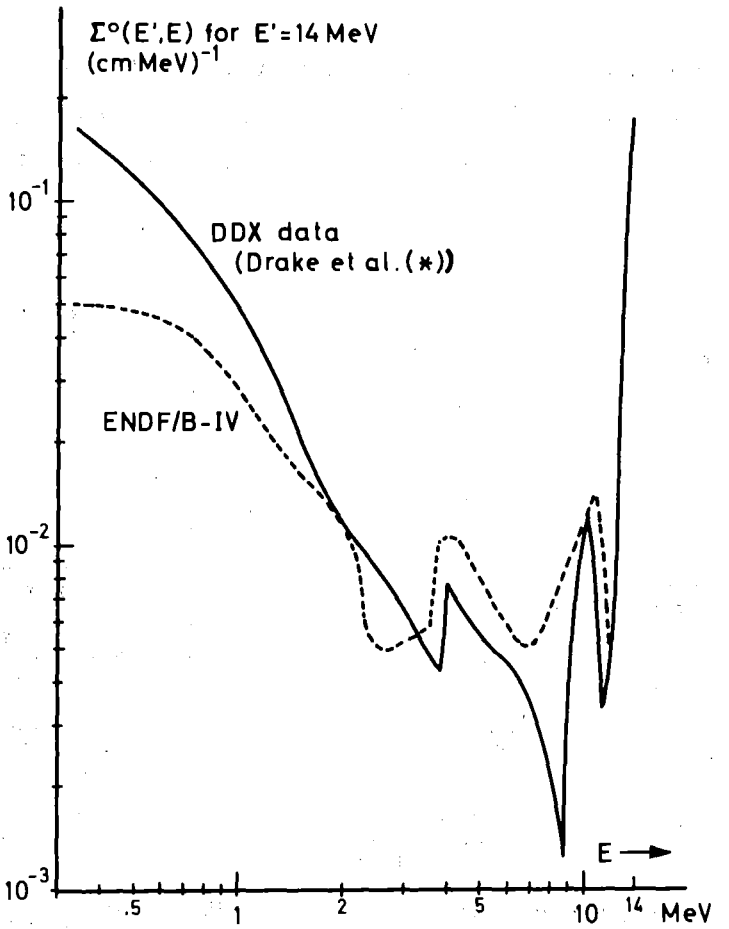

Fig. 11: Energy distribution of secondary neutrons for scattering on ^{9}Be

(*): Nucl. Sci. Eng. 63, 401 (1977)

in both isotopes. The intermediate cases of treating this change in only one of the isotopes are less interesting.

For the calculations of the neutron transport in a sphere of ^{9}Be a third version for the scattering kernel was used: The (n,2n) data were taken from ENDF/B-IV and treated along the Ii-route to produce the c.m.-to-lab. system tranformation for the secondary neutrons. This is made to replace the calculation with preliminary data in ref. /6/.

The shell source was located at r = 8 cm, the source spectrum was the spectrum of the experiment ref. /5/, for the same reasons as in ref. /6/.

5.2 ^{9}Be Sphere results

Fig. 12 presents calculated scalar neutron spectra in a sphere of ^{9}Be with 20 cm outer radius and 8 cm radius of the inner void region. The spectra are drastically different. As already stated in ref. /6/ the c.m.-to-lab. system

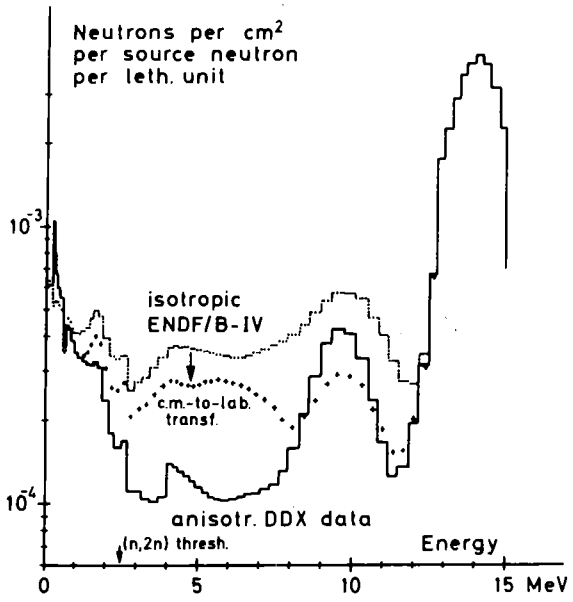

^{9}Be-sphere, 20 cm outer, 8 cm inner radius: effect of the (n,2n) anisotropy on the scalar neutron spectrum at r = 8.25 cm

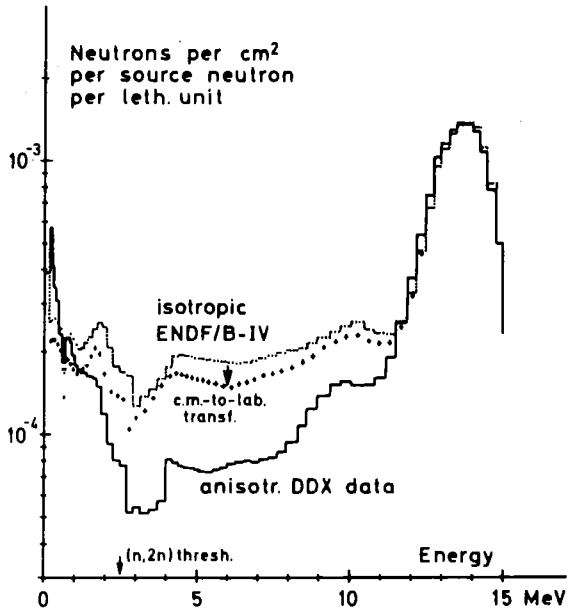

^{9}Be-sphere, 20 cm outer, 8 cm inner radius: effect of the (n,2n) anisotropy on the scalar neutron spectrum at r = 14.25 cm

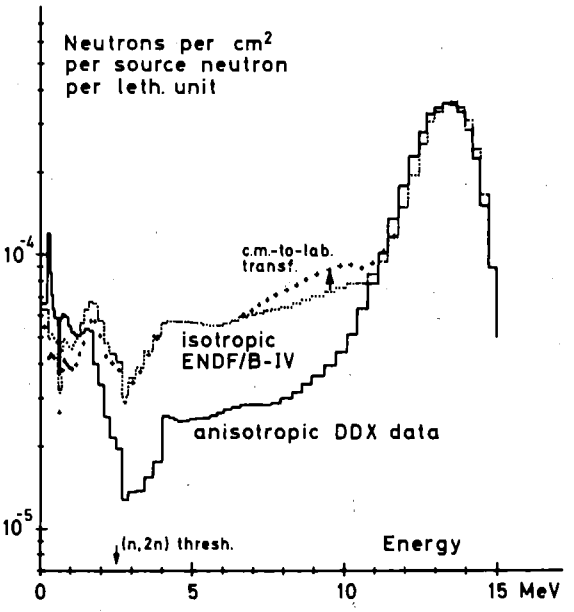

^{9}Be-sphere, 20 cm outer, 8 cm inner radius: effect of the (n,2n) anisotropy on the scalar neutron spectrum at r = 19.75 cm

Fig. 12:

transformation plays an important role in the problem. The results for the (n,2n) reaction rate are shown in Fig. 13. Again large differences are

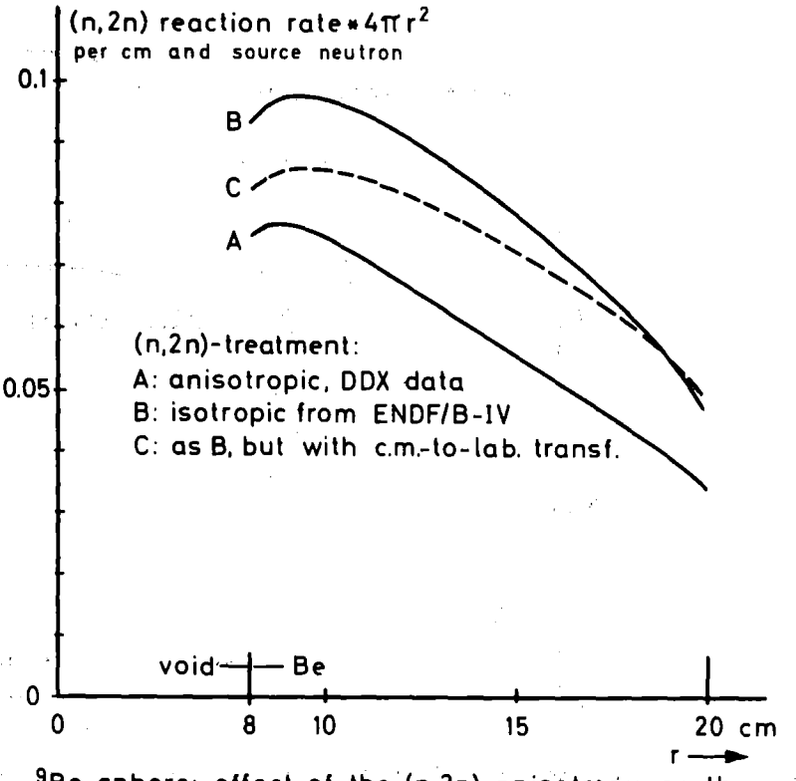

^{9}Be-sphere: effect of the (n,2n) anisotropy on the radial distribution of the (n,2n) rate

Fig. 13:
upper: new results,
lower: corrected version of Fig. 27 a of ref. /6/. Though the secondary neutron distribution has been just presumed, the relative effect of the c.m.-to-lab.-system transf. is not much different from the newer result.

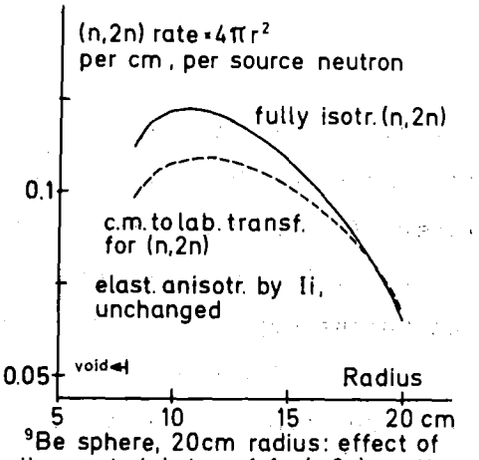

^{9}Be sphere, 20cm radius: effect of the c.m. to lab. transf. for (n,2n) scatt., (n,2n) by evaporation, nucl. temp. taken from ^{7}Li(n,n'α)

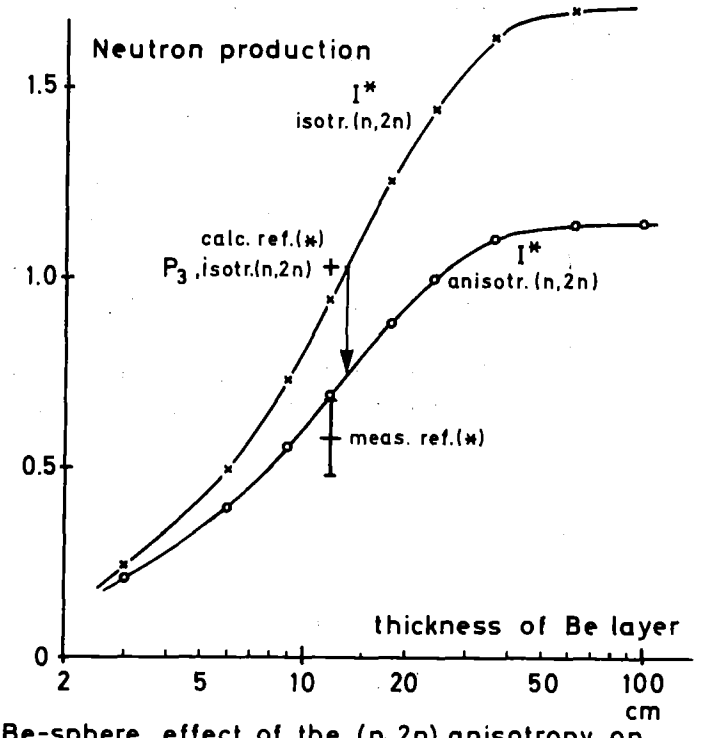

Fig. 14: Be-sphere, effect of the (n,2n) anisotropy on the neutron production, calc. with I*-method, ref.(*): T.K.Basu et al., Nucl. Sci. Eng. 70, 309 (79) different assembly

found between the various results. Fig. 14 shows the results for the neutron multiplication M inside a spherical Be layer[+)] as a function of the thickness of the layer. To compare this with the results of ref. /3/ we need a transformation for the different geometries and the difference in the assemblies. We adopt a technique employed in fission reactor calculations: The upper curve in Fig. 14 is calculated with the same nuclear data for ^{9}Be as have been used in ref. /3/. Therefore we select a point on this curve to normalize both results.

+) The multiplication is defined as for a fission reactor: $M = 1/(1-k_{eff})$.

From ref. /3/ we take the value M = 2.03 for their thickness of the Be layer. On our curve this value is given at a thickness of 13.5 cm. If we go from this point down to the second curve for the results obtained with anisotropic nonelastic data, we come with M = 1.75 much closer to the measured value of ref. /3/, which is M = 1.58 $\pm$ 0.1.

5.3 Sphere of ^{9}Be and ^{7}Li mixture

The kernel for these calculations was produced by combining the individual data by means of the code NIMIX. With the calculations for the Be-Li mixture we intended to investigate, how the tritium breeding in Flibe /18/ is affected by the scattering kernel differences. Lacking data of fluorine we took only ^{9}Be and ^{7}Li in the atomic densities of Flibe, which are $0.018 \cdot 10^{24}$ atoms/cm^{3} for either isotope.

Fig. 15 presents calculated average spectra of the scalar neutron flux in a sphere of the ^{9}Be-^{7}Li mixture with 38 cm outer radius and 8 cm radius of

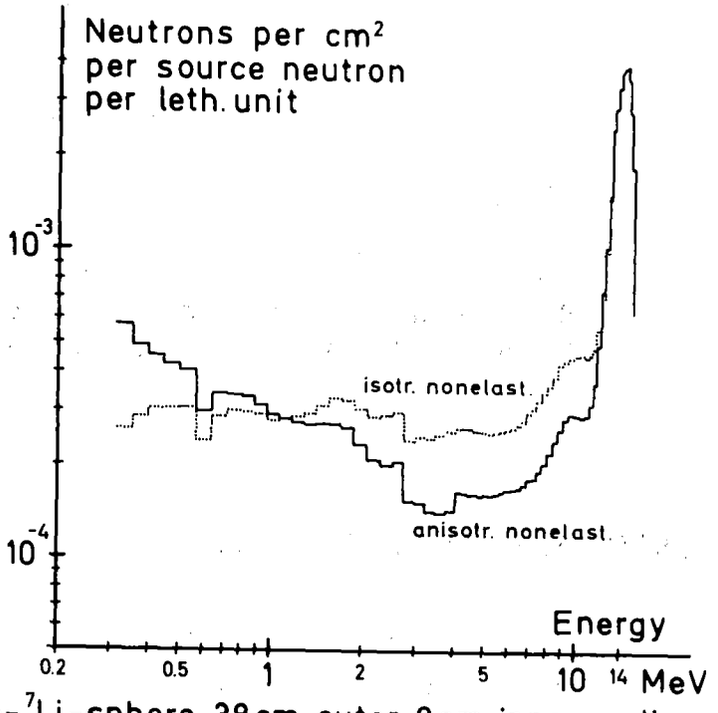

Fig. 15: ^{9}Be-^{7}Li-sphere, 38cm outer, 8cm inner radius: effect of the nonelastic anisotropy on the average scalar neutron spectrum (vol.-aver.)

the inner void for the two kernels with either isotropic or anisotropic nonelastic scattering. Taking these neutron fluxes for reaction rate calculations we find a change of about -15 % for $^{7}Li(n,n'\alpha)T$ and +15 % for $^{6}Li(n,\alpha)T$ referred to the isotropic nonelastic data. The figure for ^{6}Li may not be taken too seriously, because the fully anisotropic data are only estimated below 0.4 MeV, but the sign of the effect should be kept in mind.

Fig. 16 shows the effect of the anisotropy of the nonelastic scattering on some reaction rates as a function of the radial coordinate in the sphere of the above Be-Li mixture. The values for $^{6}Li(n,\alpha)T$ were included with the restrictions mentioned above.

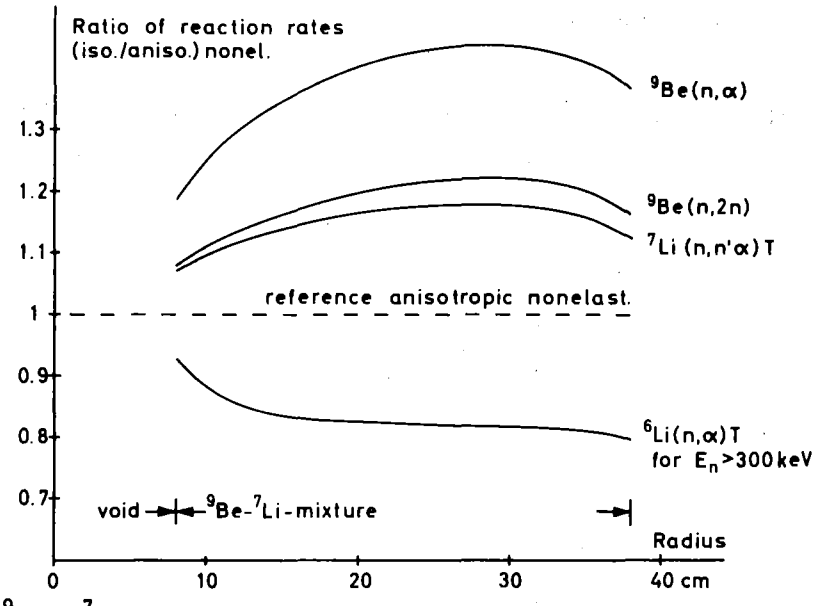

Fig. 16: ^{9}Be-^{7}Li-sphere: radial dependence of the effect of the nonelastic anisotropy on reaction rates

5.4. ^{7}Li sphere with inner ^{9}Be multiplier

With this calculation we intended to investigate, how the tritium breeding is affected if the thickness of the Be layer is varied. Again only the cases of either isotropic or anisotropic nonelastic scattering in both isotopes were considered. The assembly under consideration had an outer radius of 1.28 m, an outer ^{7}Li zone of 90 cm constant thickness and a Be layer of variable

thickness (radius of the Be-Li interface 38 cm). The source was a point source in the center of the sphere.

Fig. 17 presents the effect of the variation of the Be layer thickness on the tritium breeding in ^{7}Li. This reaction rate is monotonically decreasing with the thickness of the Be layer, so the gain in the total breeding ratio relies entirely on the increase of the reaction ^{6}Li (n,α) T.

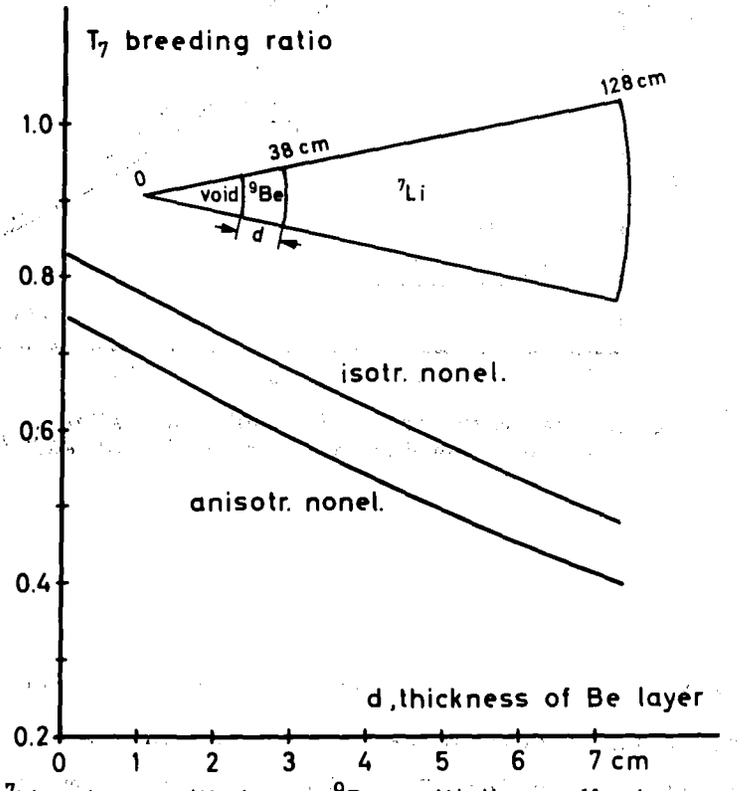

Fig. 17: ^{7}Li-sphere with inner ^{9}Be multiplier, effect of the nonelastic anisotropy on tritium breeding by $^{7}Li(n,n'\alpha)T$

In Fig. 18 the effect of the anisotropy of the nonelastic scattering on the tritium breeding in ^{7}Li is shown for a very thick layer of ^{7}Li and a Be multiplier of 4.5 cm thickness. We expected that the sign of the effect would change at greater distance from the source, but this did not occur. The flux reduction near the source is not compensated. Furthermore, the reduction of T-breeding at higher energies is not compensated by breeding at lower energies in ^{6}Li, the less abundant isotope. This comes from the fact that with the anisotropic data the fraction of secondary neutrons above

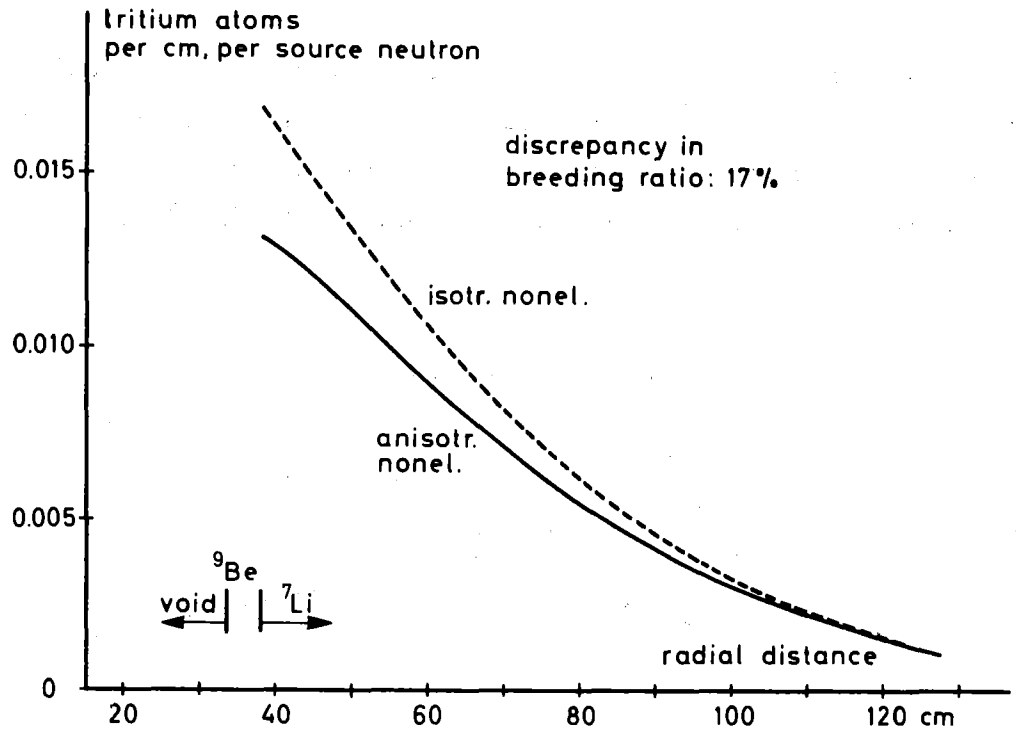

Fig. 18: ^{7}Li-sphere with inner ^{9}Be multiplier, effect of the (n,2n) anisotropy on tritium breeding by ^{7}Li(n,nα)T, rate*4πr^{2}

the threshold of ^{9}Be (n,2n) and ^{7}Li (n,n'α) is lower than with the ENDF/B-IV isotropic data. Though we have more neutrons in the lower energy part after a first interaction (see Fig. 11), the loss in multiplication by the lack of neutrons at higher energies is not compensated. So, in general for any mixture of lithium isotopes the breeding ratio of a large assembly will be lower than expected from calculations with isotropic nonelastic scattering data.

6. Consequences from the results of the test calculations

It is obvious that the uncertainty of the results is intolerable. However, open to debate is the question how to procede. Of course, the traditional way of evaluating nuclear data into single-differential data can be used to solve the problem up to a certain degree of accuracy, but by the example of beryllium it can be seen that this is no longer the best way for fusion neutronics.

From ref. /8/ it follows clearly that it is no longer allowed to describe the (n,2n) process in ^{9}Be by a "first neutron", which is scattered with excitation of discrete levels,and a "second neutron", for which an energy and angular distribution is given. Only a fraction of the "first neutron" can be treated with the kinematics of inelastic level scattering. Therefore at least one additional reaction channel must be introduced. Furthermore, the kinematics of the emission of the "first neutron" are coupled to the kinematics of the second emission and therefore this channel has to be treated twice for the coupling to each channel for the "first neutron". So, though in principle possible, the method to employ more and more reaction channels for the description of an interaction, in order to save the single-differential data base, becomes ineffective.

The double-differential data base - even if only available for particular reaction channels like in the ^{9}Be case - avoids all the difficulties of classifying scattering data into partial data, for which defined kinematics can be given. This does not only apply for the (n,2n) reaction, but also for (n,n'γ), (n,n'p), (n,n'α), (n,n't), etc. Especially in the (n,n'γ) reaction we face these difficulties already in the Ii-method, where the treatment of the continuum scattering cannot really be regarded as appropriate. In the neutron transport problem it does not matter, wether the outgoing neutrons belong to a certain reaction channel, because we need only particle currents before and after the passage of the scattering center. Distinguishing between "direct", "preequilibrium", and "compound" neutrons may serve for a theoretical interpretation of the interaction in the nucleus, but for the transport calculation these distinctions do not matter. In a multiparticle break-up we are unable to formulate the kinematics as simple as for the scattering of a single particle, if at all.

When investigating the uncertainty of transport calculations, the systematic error sources can be grouped in the following way:

i) geometric simplification in the transport calculation (divergence term)
ii) approximative treatment of the scattering kernel in the transport calculation (collision source term)
iii) use of single-differential data in the transport calculation (reconstruction of DDX data)
iv) unknown covariances

In the present form of uncertainty analysis by means of the sensitivity studies /19/ not all of the error sources could be taken into account. This caused that very often results obtained with this method were not taken seriously. In fact, in said reference errors of all four types concern the imperfectness of the tools for the realization of the method, whereas the mathematical basis of the method is not affected.

Commonly, errors of type (i) are investigated independently. This is only an approximation, because it has some correlation with errors of the other types. A three-dimensional Monte-Carlo-calculation, even with rigorous scattering kernel treatment like in /20/ fails to predict effects, if the target volumes under consideration become small. To investigate smaller effects and for investigations in systems studies two-dimensional S_N calculations are required, however, with higher angular resolution near to a preferred direction /5/ than presently available.

The present paper deals with the error sources of types (ii) and (iii). Having established a method to eliminate errors from these sources down to the level of the discretization errors, attention should be concentrated on errors of type (iv). The naive method of introducing "plausible" changes into double-differential data can certainly not account for the complex partial error compensation in the error propagation process. Therefore we propose the use of double-differential data together with their covariance data in a rigorous sensitivity study by means of the rigorous I^*-method for the transport calculational part of the problem.

7. Conclusions

The I^*-method as described in KfK 2832, Part I, was realized within the NITRAN code system. By this method neutron transport calculations can be performed, in which a rigorous treatment of the anisotropic scattering kernel provides an undisturbed microscopic neutron balance equation. Double-differential cross section data make the I^*-method independent of assumptions about the physics of the scattering. A smooth transition from single-differential data to this data type is provided in the I^*-route of the NITRAN system.

By means of test calculations for some assemblies related to the neutronics of a fusion reactor we demonstrate the important effects associated with the anisotropy of the nonelastic scattering. It was shown that introducing the treatment of this anisotropy into the transport calculations is more than just another approximation: the element of rigour, which is introduced with the Ii-method, is also introduced for the nuclear data part of the problem by demanding double-differential cross sections in the form of a total neutron emission cross section in the lab. system. Though in Appendix 3 of KfK 2832, Part I, we can see, that the P_L method can be used also for double-differential data, we do not see the necessity to develop such a method in addition to the existing I^*-method. Currently used P_L calculations require kinematics for the partial single-differential data and so does the Ii-method. From this point of view the Ii-method is not completely rigorous as is the I^*-method.

Since the I^*-method is not directly comparable to other methods, its relation to the Ii-method can be used to appreciate the high calculational speed of the method. If double-differential data are available the scattering kernel matrix generation shrinks to an interpolation problem in connection with some flux-weighted averaging. For the solution of the S_N equations any method can be used, and therefore it is advisable to adapt existing S_N codes also for the use of the I^*-method.

With respect to the conclusions of Part I the following work remains to be done:

a) S_N codes for cylindrical, two-dimensional and three-dimensional geometry must be developed.

b) A Monte-Carlo code should incorporate the I^*-method.

c) Codes for uncertainty analysis by means of the sensitivity study method with use of the I^*-method for the transport calculation part of the problem should be developed.

d) Double-differential neutron emission cross section data must be evaluated together with their covariances.

e) Both the Ii- and the I^*-method should be applied also to transport calculations for other particles than neutrons.

Acknowledgement

The authors thank Prof. K. Wirtz, Dr. G. Keßler and DP M. Küchle for their invarying support. We are indebted to Mr. J. Yamamoto (Osaka University) and Dr. H. Iida (JAERI) for their help in providing processed (n,2n) data for ^{9}Be from ENDF/B-IV.

One of the authors (A.T.) wishes to thank the Alexander-von-Humboldt-Stiftung for financially supporting his stay in the Institut für Neutronenphysik und Reaktortechnik of the Kernforschungszentrum Karlsruhe.

References

/1/ K.D. Lathrop
"DTF-IV, A FORTRAN-IV Program for Solving the Multigroup Transport Equation with Anisotropic Elastic Scattering"
LA-3373 (1965)

/2/ H.W. Wiese
"Verbesserte Behandlung der anisotropen elastischen Neutronenstreuung durch konsistente Transportnäherungen energieabhängiger Ordnung"
PhD thesis, KfK 2377, Karlsruhe (1976)

/3/ T.K. Basu, V.R. Nargundkar, P. Cloth, D. Filges, and S. Taczanowski
"Neutron Multiplication Studies in Beryllium for Fusion Reactor Blankets"
Nucl. Sci. Eng. 70, 309 (1979)

/4/ M. Ebisuya, H. Maekawa, Y. Seki, A. Takahashi, J. Yamamoto
"A Study on the Neutron Transport Code Systems for Fusion Reactor Design"
JAERI-M 8135 (1979)

/5/ H. Bachmann, U. Fritscher, F.W. Kappler, D. Rusch, H. Werle, H. W. Wiese
"Neutron Spectra and Tritium Production Measurements on a Lithium Sphere to Check Fusion Reactor Blanket Calculations"
Nucl. Sci. Eng. 67, 74 (1978)

/6/ A. Takahashi, D. Rusch
"Rigorous Methods of Anisotropic Neutron Transport Calculations and the NITRAN System for Fusion Neutronics Applications"
KFK 2832, Part I, (1979)

/7/ Summary Report of the IAEA Advisory Group Meeting on Nuclear Data for Fusion Reactor Technology, Vienna, 11-15 Dec. 1978, ed. by A. Lorenz and D.W. Muir, INDC (NDS)-101/LF (1979)

/8/ D.M. Drake, G.F. Auchampaugh, E.D. Arthur, C.E. Ragan, P.G. Young
"Double-Differential Beryllium Neutron Cross Sections at Incident Energies of 5.9, 10.1, and 14.2 MeV"
Nucl. Sci. Eng. 63, 401 (1977)

/9/ F.G. Perey
"Neutron total, elastic and inelastic scattering and gamma-ray production data"
Inv. Paper for the IAEA Advisory Group Meeting on Nuclear Data for Fusion Reactor Technology, Vienna, 11-15 Dec. 1978, to be published by IAEA

/10/ P. Barbucci, F. Di Pasquantonio
"Exponential Supplementary Equations for S_N Methods: The One-Dimensional Case"
Nucl. Sci. Eng. 63, 179 (1977)

/11/ P. Barbucci, F. Di Pasquantonio
"Exponential Supplementary Equations for S_N Methods: The Two-Dimensional Case"
Proc. 5th Conf. on Reactor Shielding, April 18-23, Tennessee, USA, (1977)

/12/ C. Guenther
"IPOL-Ein FORTRAN-Programm zur zweidimensionalen Interpolation"
KFK 2175 (1975)

/13/ J.P. Odom and J.K. Shultis
"Anisotropic Neutron Transport Without Legendre Expansions"
Nucl. Sci. Eng. 59, 278 (1976)

/14/ B. Goel
"Graphical Representation of the German Nuclear Data Library KEDAK, Part 1"
KFK 2233 or NEANDC(E) 170 "U" (1975)

/15/ P. Cloth, D. Filges, R. Herzing, N. Kirch
"Neutron Multiplication Effect of CTR Blankets Containing Beryllium"
Proc. 9th Symp. on Fusion Technology (SOFT), Garmisch-Partenkirchen, Fed. Rep. of Germany, June 14-18, (1976)

/16/ A. Hasegawa
(to be published as JAERI-report)

/17/ R.Q. Wright, N.M. Greene, J.L. Lucius, C.W. Craven, Jr.
"SUPERTOG, a Program to Generate Fine Group Constants and P_N-Scattering Matrices from ENDF/B"
ORNL-TM-2679 (1969)

/18/ M.A. Abdou and R.W. Conn
"A Comparative Study of Several Fusion Blanket Designs"
Nucl. Sci. Eng. 55, 256 (1974)

/19/ S.A.W. Gerstl, D.J. Dudziak, and D.W. Muir
"Cross-Section Sensitivity and Uncertainty Analysis with Application to a Fusion Reactor"
Nucl. Sci. Eng. 62, 137 (1977)

/20/ J. Yamamoto, A. Takahashi, M. Ebisuya, and K. Sumita
"Measurements of Angular Flux Spectra Emitted from Lithium and Graphite Slabs with the D-T Neutron Source"
To be published (J. Nucl. Sci. Techn.)

Appendices: Improvements in the NITRAN System

Appendix 1: NIKER

The kernel outputs were changed from parallel output of level and continuum kernels to a single output, which is stored in FI. This reduces the required storage area.

The isotropic part of the scattering kernel is transfered directly to the S_N codes, if the input parameter ICON = 0. For ICON = 1 the matrix FI contains the complete kernel.

Of course, the input of NITRAN-S was modified to accept the new format of the kernel. The other S_N codes are coupled to NIMIX.

Appendix 2: NIMIX

This code produces "mixed-isotope" kernels and/or kernels in the order of the layers in an assembly with several material zones. NIMIX contains two subroutines, MONMIX and MULMIX. The former is to produce mixed-isotope kernels for a single layer of homogeneous material, then the latter arranges them in the order of the material layers in the assembly.

NIMIX accepts the outputs from both NIKER in the Ii-route and ANIKER in the I*-route to produce kernels for one-dimensional transport calculations.

We do not claim that the code NIMIX is programmed elegantly, it should be revised for technical use. Fig. A 1 shows the flow chart of NIMIX.

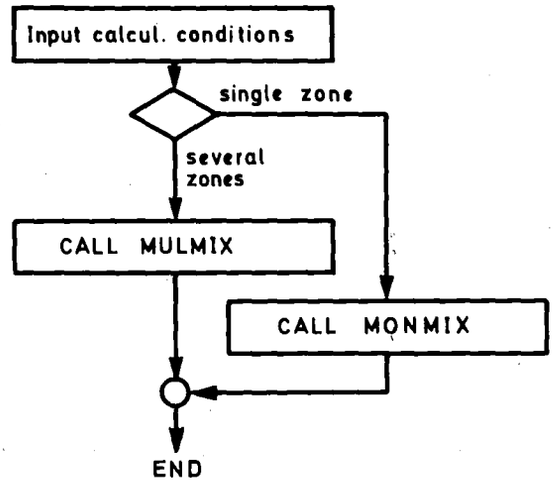

Fig. A 1: Flow chart of NIMIX

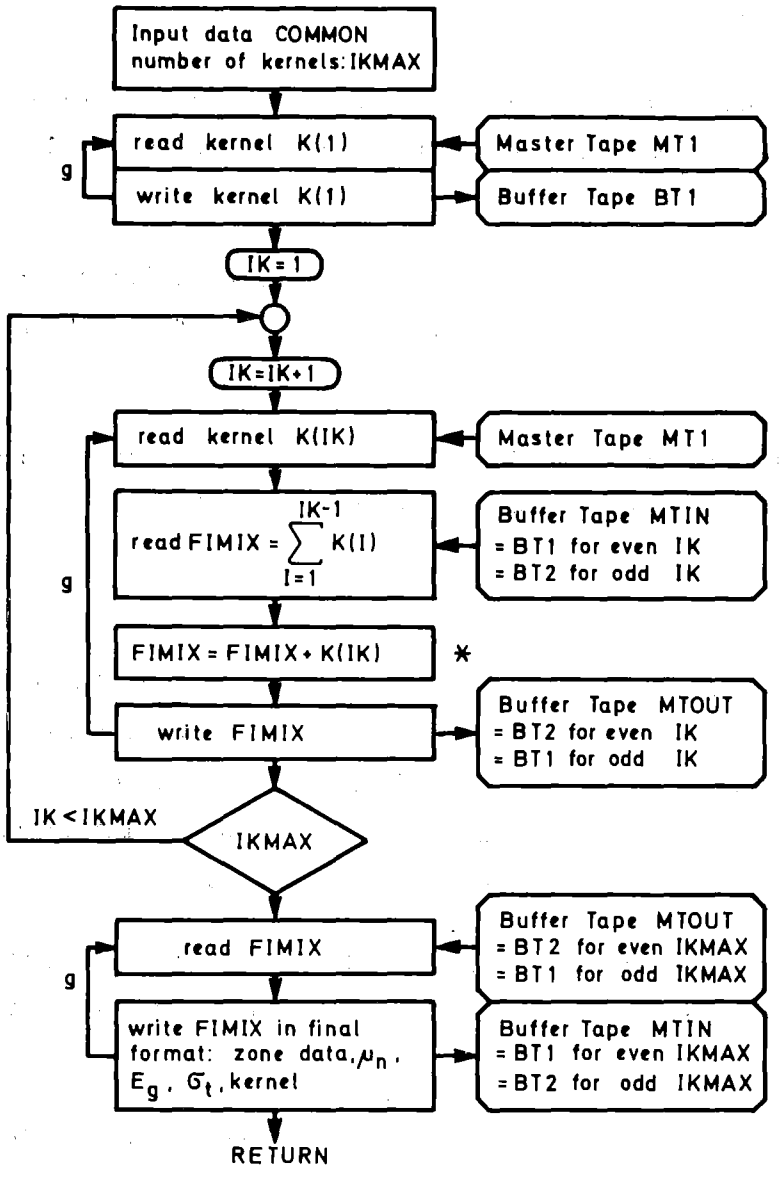

Fig. A 2: Flow chart of subroutine MONMIX in NIMIX

Fig. A 2 presents the flow chart of the subroutine MONMIX. Reading and writing is straightforward from magnetic tapes to magnetic tapes. Several tapes are employed for input or output, therefore the related unit numbers MTIN and MTOUT are switched according to the requirements.

The flow chart of MULMIX differs from MONMIX only slightly, and in Fig. A 2 the points at which both soubroutines differ, are marked by (*). In MULMIX the kernels are not added, but arranged in the sequence of the material zones for each sink group.

Appendix 3: NITRAN-MS

This is the extension of the code NITRAN-S for spherical assemblies with several material zones. NITRAN-MS receives the cross section data from NIMIX. At present NITRAN-MS accepts up to 5 material zones. For calculations for a single material zone the code NITRAN-S is left in operation.

Appendix 4: NITRAN-MP

This S_N code solves the transport problem for a one-dimensional plane assembly. Up to 5 material zones are accepted. The basic difference equation is

$$\mu_n\left[f_g(m+\tfrac{1}{2},n)-f_g(m-\tfrac{1}{2},n)\right]+\sigma_t^g\cdot\Delta x_m\cdot f_g(m,n)=\Delta x_m\left[C_g(m,n)+S_g(m,n)\right] \quad \text{(A-1)}$$

where $f_g(m+1/2,n)$, $f_g(m-1/2,n)$, and $f_g(m,n)$ are angular fluxes at the spatial boundary points and the central one, respectively. C_g is the collision source expressed by the Ii- or $I^{\pm}$-formalism, and S_g the external source.

Both the linear and the exponential method (LM and EM) are used to generate the supplementary equations. Option parameter is LORE.

Exponential method (LORE = 0):

The assumption is, /10/:

$$\left[f_g(m,n)\right]^2 = f_g(m+\tfrac{1}{2},n)\cdot f_g(m-\tfrac{1}{2},n) \quad \text{(A-2)}$$

Substituting Eq. (A-2) into Eq. (A-1) we obtain the following equation, which gives successive solutions for the $f_g(m,n)$ starting from the flux values at the boundaries ("inner iteration loop"):

$$f_g(m,n) = \frac{1}{2}\left(-A+\sqrt{A^2+4B}\right) \quad \text{(A-3)}$$

with

$$A=\frac{\sigma_t^g\,\Delta x_m}{|\mu_n|}\cdot f_i \quad \text{(A-4)}$$

$$B = f_i\left[f_i+\frac{\Delta x_m}{|\mu_n|}\cdot\left(C_g(m,n)+S_g(m,n)\right)\right] \quad \text{(A-5)}$$

where

$$f_i = f_g(m-\tfrac{1}{2},n) \text{ for } \mu > 0\,, \quad f_i = f_g(m+\tfrac{1}{2},n) \text{ for } \mu < 0 \tag{A-6}$$

The first iteration is always executed with the LM, and at the boundaries LM is to be used in all iterations, because in both cases the flux values can be zero systematically. Furthermore, the program switches to the LM, if the flux values are less than 10^{-30}. Thus also numerical difficulties by accidentally very small values or zeros are avoided.

Linear method (LORE = 1):

The assumption is /1/:

$$f_g(m,n) = \frac{1}{2}\left[f_g(m+\tfrac{1}{2},n) + f_g(m-\tfrac{1}{2},n)\right] \tag{A-7}$$

Substituting Eq. (A-7) into Eq. (A-1) we get

$$f_g(m,n) = C \cdot f_i + D\left[C_g(m,n) + S_g(m,n)\right] \tag{A-8}$$

with

$$C = 2\,|\mu_n| \cdot D/\Delta x_m \tag{A-9}$$

$$D = \Delta x_m / \left[2\,|\mu_n| + \sigma_t^g \Delta x_m\right] \tag{A-10}$$

where the f_i are given as in (A-6).

For the negative flux correction the same strategy as in ref. /6/ was applied, which means that a negative flux correction is programmed as a fix-up at zero, but it is not used, because the rigorous methods diminish the problem drastically by the non-negative collision source term.

The exponential method yields higher calculational speed, though the supplementary equations are more complicated, because a larger spatial mesh size can be applied. For a fine mesh size the result with the EM must be close to the result with LM, because the assumption (A-2) for the EM can be approximated by the assumption (A-7) for the LM, if the differences between the f_g are small.

The source term ($C_g + S_g$) is treated in the same manner as in NITRAN-S (and -MS). The flow chart of NITRAN-MP differs only slightly from that of NITRAN-S: The iteration starts at the source boundary and three subroutines are added for various options to estimate the effect of the transverse leakage, steered by the option parameter LEAK. For LEAK = 0 no correction is made, LEAK = 1, 2, and 3 are used to call the subroutines FLEAK1, FLEAK2, and FLEAK3, respectively. FLEAK1 produces the usual diffusion approximation (buckling correction). This approximation, however, fails for the cases, where the collision frequency is so small, that the fluxes are strongly anisotropic.

In subroutine FLEAK2 the diffusion approximation is adjusted to account for the anisotropy of the flux. It uses the effective total cross section

$$\Sigma_{eff}(x,E) = \Sigma_t(E) + \eta(x,E) \cdot D(E) \cdot B_\perp^2 \qquad \text{(A-11)}$$

where D(E) is the diffusion coefficient at $B_\perp^2$ the transverse buckling. The function $\eta(x,E)$ is a trial function for the adjustment, which is $\eta = 1$ for isotropic flux and $\eta = 0$ for purely forward or backward flux. A first attempt to determine values for $\eta(x,E)$ relies on the assumption, that the transverse component of the flux-weighted average of the flux, which is

$$\bar{\mu}(x,E) = \int_{-1}^{+1} \mu \cdot f(x,\mu,E)\, d\mu \Big/ \int_{-1}^{+1} f(x,\mu,E)\, d\mu \qquad \text{(A-12)}$$

can be used to estimate

$$\eta(x,E) = \left[1 - (\bar{\mu}(x,E))^2\right]^{1/2} \qquad \text{(A-13)}$$

In the averaging the angular fluxes of each iteration step can be used. This means, that this correction is included in the iteration process, as opposed to an initial energy-dependent buckling.

We intend to replace the exponent (1/2) in Eq. (A-13) by a fitting parameter a, the value of which is adjusted by means of a separate Monte-Carlo calculation /20/.

Actually, FLEAK2 relies on an initial flux guess (NGUESS = 1) in the input for NITRAN-MS, but this can be bypassed by some additional statements.

The third subroutine FLEAK3 uses an effective transverse leakage that is estimated by means of the non-collision probability p_{non} for a neutron that flies from the x-axis to the transverse surface of the assembly. For a cylindrical slab assembly this is estimated as

$$p_{non}(x,\mu,E) = e^{-\sigma_t(x,E)\cdot\frac{R}{\sqrt{1-\mu^2}}} \quad \text{for } \mu_1 \le \mu \le \mu_2 \tag{A-14}$$

with R = radius of the assembly, and μ restricted to those radius vectors which point to the transverse surface. Within this angular interval p_{non} is averaged to give the transverse leakage $L_\perp(x,E)$ weighted with the angular fluxes:

$$L_\perp(x,E) = \int_{\mu_1(x,E)}^{\mu_2(x,E)} p_{non}(x,\mu,E)\cdot f(x,\mu,E)\,d\mu \Big/ \int_{-1}^{+1} f(x,\mu,E)\,d\mu \tag{A-15}$$

The effective transverse leakage cross section is then

$$\sigma_\perp(x,E) = \sigma_t(E)\cdot\frac{L_\perp(x,E)}{1-L_\perp(x,E)} \tag{A-16}$$

In the S_N difference equation the effective total cross section $(\sigma_t(x,E) + \sigma_\perp(x,E))$ is used insted of $\sigma_t(x,E)$. This procedure is most promising for the cases in which the collision frequency in the x-direction is small. This may be another way to produce an estimate for the parameter a in FLEAK 2.

Fig. A 3 shows results for the various transverse leakage approximations.

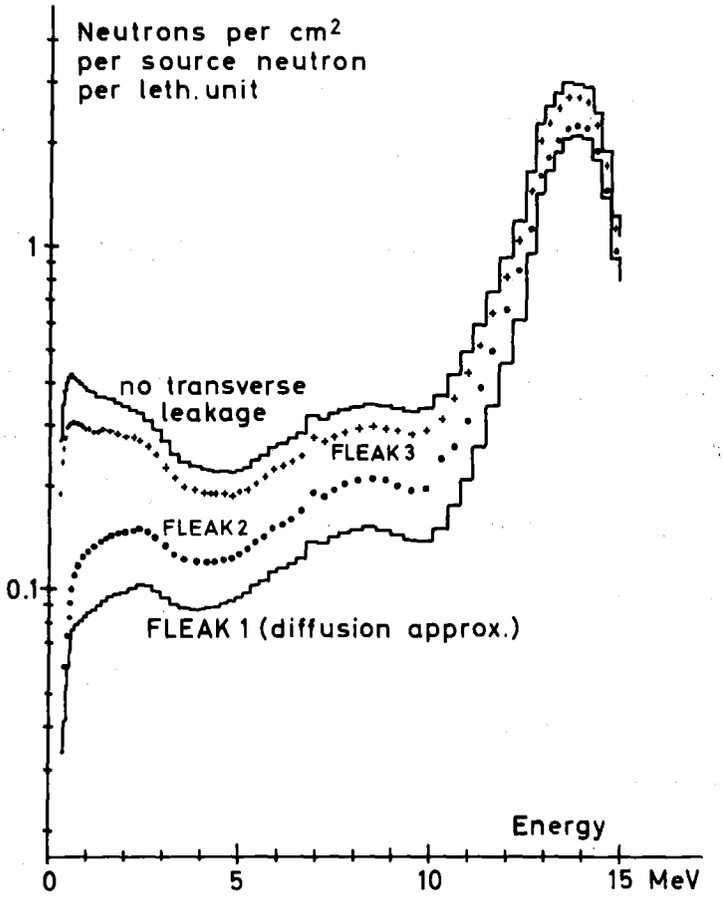

Fig. A 3: ^{7}Li-slab: effect of various transverse leakage approximations on the average scalar flux

Appendix 5: Failure of the exponential method for spherical geometry

We attempted to introduce the exponential method (EM) to generate the supplementary equations to the S_N equations. The supplementary equation for the EM in the spherical geometry is /10/:

$$f_g(m,n) = \frac{-\sigma_t^g \cdot V_m + \left[(\sigma_t^g \cdot V_m)^2 + 4\,G\,H\right]^{1/2}}{2\,G} \qquad \text{(A-17)}$$

where

$$G = \frac{|\mu_n| \cdot A^*}{f_{im}} + \frac{\alpha_{n+1/2}}{W_n \cdot f_{in}} \qquad \text{(A-18)}$$

$$H = |\mu_n| A^{**} f_{im} + \frac{\alpha_{n-1/2}}{W_n} f_{in} + \left[C_g(m,n) + S_g(m,n)\right] \cdot V_m \qquad \text{(A-19)}$$

with

$$\left.\begin{aligned} f_{in} &= f_g(m, n-1/2) \qquad \text{(first index "i" for "initial")} \\ f_{im} &= f_g(m+1/2, n) \text{ for } \mu < 0;\ f_{im} = f_g(m-1/2, n) \text{ for } \mu > 0 \\ A^* &= A_m \text{ and } A^{**} = A_{m+1} \text{ for } \mu < 0 \\ A^* &= A_{m+1} \text{ and } A^{**} = A_m \text{ for } \mu > 0\,. \end{aligned}\right\} \qquad \text{(A-20)}$$

The other quantities are defined in ref. /6/, section 3. In ref. /10/ A^* is used at the place of A^{**}. This was one of the causes for the trouble reported in ref. /6/.

For the starting angle an additional supplementary equation is used /10/. Within an iteration step the f_{in} and f_{im} are the angular fluxes at the boundaries, from which the solution of the difference equation procedes to generate the central flux value $f_g(m,n)$, from which by the starting assumption the fluxes at the opposite boundaries are generated, i. e.

$$\left.\begin{aligned} f_{fn} &= \frac{\left[f_g(m,n)\right]^2}{f_{in}} \qquad \text{(first index "f" for "final")} \\ f_{fm} &= \frac{\left[f_g(m,n)\right]^2}{f_{im}} \end{aligned}\right\} \qquad \text{(A-21)}$$

where
$$\left.\begin{aligned} f_{fn} &= f_g(m, n+\tfrac{1}{2}) \\ f_{fm} &= f_g(m-\tfrac{1}{2}, n) \quad \text{for } \mu < 0 \\ f_{fm} &= f_g(m+\tfrac{1}{2}, n) \quad \text{for } \mu > 0. \end{aligned}\right\} \qquad \text{(A-22)}$$

As stated in ref. /10/ at the boundaries and in the first iteration, when systematically fluxes can be zero, the linear interpolation method (LM) must be used. Furthermore. the program switches to LM, if the flux values are less than a small positive value, e. g. 10^{-30}.

Of course, the first trials with the EM were made with the same radial mesh as for the pure LM calculation. A result is shown in Fig. A 4. The scalar fluxes obtained with the EM are not close to the result of the pure LM calculation. The reason for this difference is illustrated in Fig. A 5, which shows angular fluxes near the monoenergetic and localized source in the problem. The presumed nearly exponential dependences of the fluxes on both radius and angle are simply not true for this case. The linear interpolation is also only a crude assumption to generate the supplementary equations, but it behaves numerically good-natured and leads at least to fast convergence, whereas the EM converges slowly, if at all.

In the next approach to save the EM for that part of the problem, where the assumptions about the flux shape are more realistic, we inserted statements to switch to the LM, if the ratio of the fluxes to be interpolated exceeds a certain limit, i. e. two, or even only one order of magnitude. However, even with this restriction the EM failed to converge as rapid as the LM. Therefore with additional statements in the innermost iteration loop and the slow convergence, the EM failed to satisfy our expectations on the gain in the calculational speed by a more coarse radial mesh, at least in the outer parts of the assembly. The related statements are left in the program to facilitate further studies of this problem.

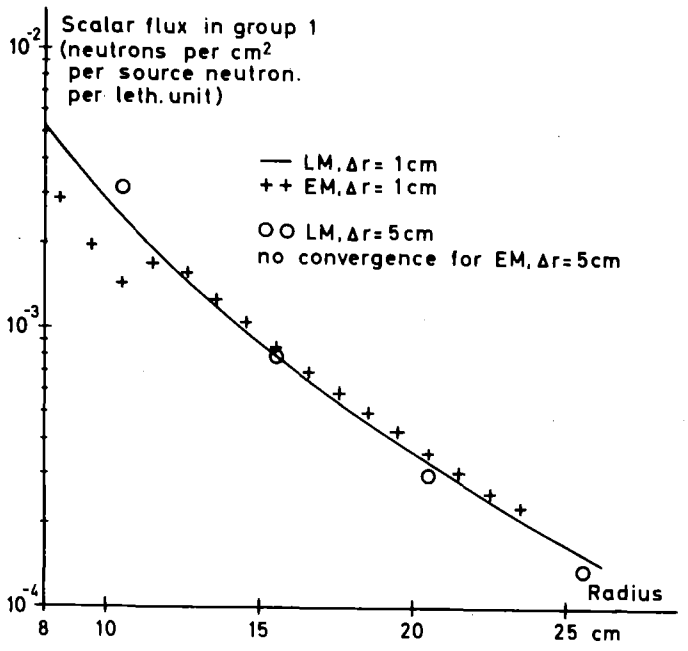

Fig. A 4: ^{7}Li sphere: test of the exponential method versus the linear method to generate the supplementary equations

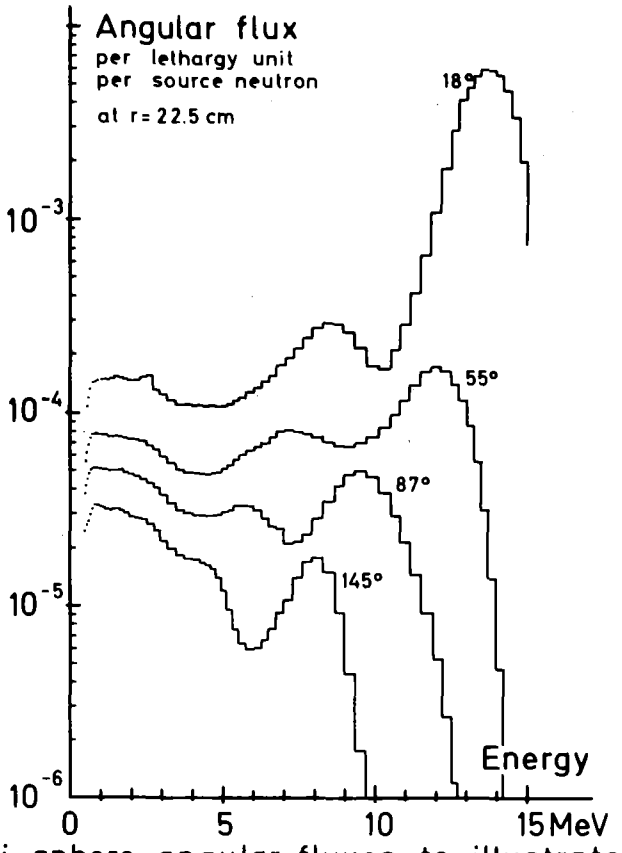

Fig. A 5: ^{7}Li-sphere, angular fluxes to illustrate the origin of the failure of the EM
(outer radius: 38 cm, inner: 8 cm; S_{19}, LM, Δr=1cm, NITRAN-S)

For fission reactor problems, where we have spatially and energetically distributed sources, the exponential method is useful, especially in connection with the rigorous Ii- and I^*-methods, which do not lead to negative collision source term problems.

Erratum in part I (ref. /6/)

Erroneously the ordinate values for Fig. 27 a have been multiplied by an additional factor of 2. Moreover, the rates are per cm, and not per cm^2, as has been drawn. The corrected version of Fig. 27 a is on page 23 of this part II, together with new results with better data.

Table 1: S_{19} μ-set

n	μ_n	w_n
1	- 0.9999	0.018775
2	- 0.9250	0.044975
3	- 0.8200	0.087875
4	- 0.5735	0.125000
5	- 0.3200	0.103375
6	- 0.1600	0.06750
7	- 0.0500	0.05250
8	0.0500	0.05250
9	0.1600	0.06750
10	0.3200	0.07250
11	0.4500	0.063375
12	0.5735	0.06250
13	0.7000	0.077875
14	0.8850	0.05625
15	0.9250	0.016515
16	0.95106	0.014950
17	0.98480	0.010985
18	0.9950	0.003775
19	0.9999	0.001275